Materialia 14 (2020) 100918

Contents lists available at ScienceDirect

Materialia

journal homepage: www.elsevier.com/locate/mtla

Solute segregation assisted superplasticity in a low-alloyed Mg–Zn–Ca–Sn–Mn alloy

Zhen-Ming Hua [b,c], Bing-Yu Wang [b], Cheng Wang [a,b,*], Hong-Min Zhang [b], Chun-Feng Du [b], Yi-Jia Li [b], Min Zha [a,b,c], Pin-Kui Ma [b], Zhi-Zheng Yang [b], Hui-Yuan Wang [a,b,c,**]

[a] State Key Laboratory of Automotive Simulation and Control, Jilin University, Changchun 130012, PR China
[b] Key Laboratory of Automobile Materials of Ministry of Education & School of Materials Science and Engineering, Jilin University Nanling Campus, No. 5988 Renmin Street, Changchun 130025, PR China
[c] International Center of Future Science, Jilin University, Changchun 130012, PR China

ARTICLE INFO

Keywords:
Superplasticity
Thermostability
Magnesium alloys
Solute segregation
Grain boundaries sliding

ABSTRACT

In this study, we are pleased to report a low-alloyed Mg–1.0Zn–0.45Ca–0.35Sn–0.2Mn (wt. %) alloy sheet fabricated by hot rolling, showing superplastic deformation ability with tensile elongation of ~410%±30% at 573 K and 1×10^{-3} s^{-1}. The superplasticity is co-dominated by grain boundaries sliding (GBS) and solute drag creep. Unlike high-alloyed Mg alloys with dispersed precipitates, this low-alloyed system keeps its fine-grained microstructure by the co-segregation of Zn and Ca atoms at grain boundaries (GBs) coupled with a few precipitates. Although the co-segregation of Zn and Ca atoms at GBs are not favored for GBS, the resulting superior thermostability is of great importance to achieve superplastic deformation. Thus, we put forward a new path in achieving superplasticity in low alloyed Mg alloys by using a complementary thermodynamic and kinetic stabilization approach.

1. Introduction

Superplastic forming has been applied to produce complex magnesium (Mg) alloy components without local thinning [1, 2]. When an initial fine-grained structure is formed, the high thermostability is required to prevent grain growth to activate grain boundary sliding (GBS) during deformation [3, 4]. Therefore, studies on superplastic deformation have been mainly focused on high-alloyed Mg alloys containing numerous precipitates to stabilize the fine grains [1, 2]. In a previous work, a fine-grained structure (~3 μm) Mg–9Al–1Zn (AZ91) sheet, decorated with dispersed spherical $Mg_{17}Al_{12}$ phase, exhibits an excellent superplasticity of ~740% at 573 K and 1×10^{-3} s^{-1} [5]. However, increasing element contents in Mg alloys makes their processing more difficult and increases the preparation cost for industries. For low-alloyed Mg alloy systems, grain coarsening is often inevitable due to reduced thermal stability, and thus superplasticity is obtained on the condition of significant grain refinement achieved by severe plastic deformation (SPD) [6, 7]. However, it is still a challenge for industries to fabricate superplastic Mg alloys by SPD due to the complicated processes. Although an elongation of ~350% was obtained in a hot-rolled Mg–3Al–1Zn–0.3Mn (AZ31) alloy sheet at 603 K [8], a considerable grain growth (from 6 μm to 11 μm), appearing after elongation of ~300%, was detrimental to further deformation. Therefore, it is of great significance to retard grain growth in low-alloyed Mg alloys to achieve superplastic deformation.

There are two basic strategies to inhibit grain growth at elevated temperatures. Kinetically, Zener pinning effect from dispersed fine precipitates or dragging force from segregated solutes can be used to slow down the migration of grain boundaries (GBs) [4, 5, 9]. Thermodynamically, solute atoms are expected to segregate at GBs and reduce the GB energy, which decreases the driving force for grain growth [9–11]. More recently, numerous studies [9, 10, 12–14] pay attention to reveal the influence of solute atoms on the thermostability of nano-/ultrafine-grained alloys, which possess a large probability for GB segregation due to extremely high excess free energy. For example, the mechanical alloyed nanocrystalline Mg–5Ti (at. %) alloy was found to exhibit substantially enhanced thermostability at 623 K, which is originated from the enrichment of Ti at GBs [13]. However, there have been few experimental reports on the thermodynamic stabilization of low-alloyed Mg alloys with fine-grained structure during deformation at elevated temperatures, due to a low density of crystalline defects and dilute alloying contents. Choi *et al.* [15] pointed out that for a given solvent, the preferred segregative solutes possess characteristics of large atomic size misfit and low bulk solubility. Therefore, some potential elements

* Corresponding author at: State Key Laboratory of Automotive Simulation and Control, Jilin University, Changchun 130012, PR China.
** Corresponding author at: International Center of Future Science, Jilin University, Changchun 130012, PR China.
E-mail addresses: chengwang@jlu.edu.cn (C. Wang), wanghuiyuan@jlu.edu.cn (H.-Y. Wang).

https://doi.org/10.1016/j.mtla.2020.100918
Received 19 April 2020; Accepted 4 October 2020
Available online 6 October 2020

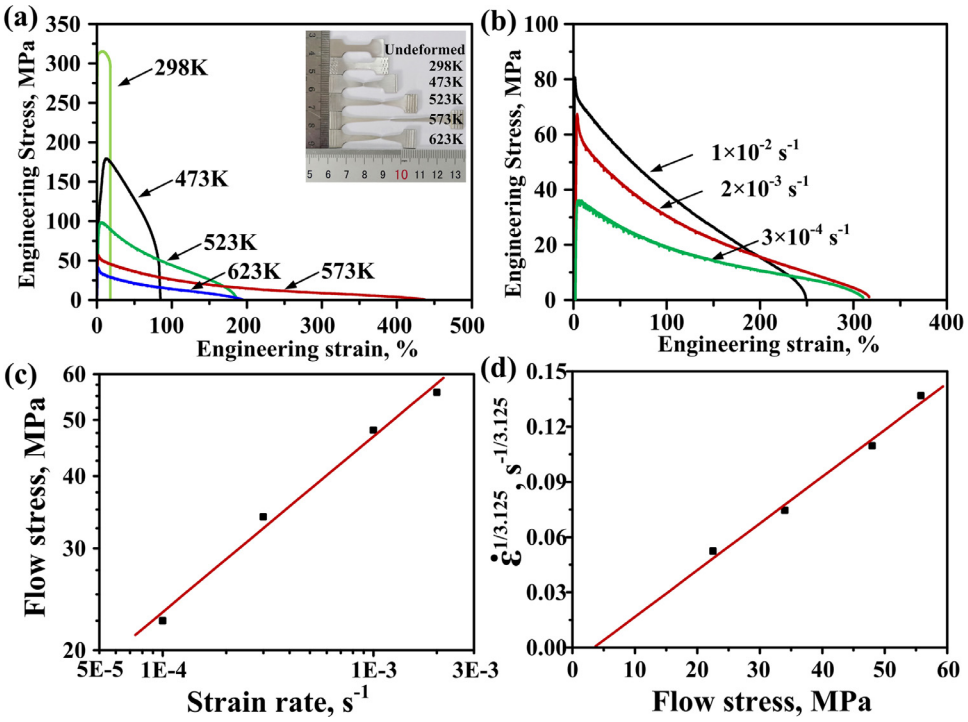

Fig. 1. (a) Tensile stress-strain curves of the rolled and annealed ZXTM1000 alloy deformed at 298 – 623 K and 1×10^{-3} s^{-1}, where the insert is the appearance of typical specimens after failure; (b) Tensile stress-strain curves of the rolled and annealed ZXTM1000 alloy deformed at 573 K and 3×10^{-4} s^{-1} – 1×10^{-2} s^{-1}; (c) variations in σ with $\dot{\varepsilon}$, showing the strain-rate sensitivity exponent (m); (d) variations in $\dot{\varepsilon}^{1/3.125}$ with σ, showing the threshold stress.

should be singled out to prepare the objective low-alloyed Mg alloy with high thermostability to achieve superplasticity.

It was reported that the Mg–Zn–Ca-based alloys would present an evident co-segregation of Zn and Ca atoms along the GBs after appropriated thermomechanical processing [16–18], even with an average grain size of ~20 μm [16]. To ensure a certain solubility of the Zn and Ca atoms for segregating to the GBs and obtain a fine-grained structure for the superplastic deformation, the temperature of thermomechanical processing and the content of alloying elements should be strictly controlled. Based on the isothermal cross-section of the Mg–Zn–Ca ternary phase diagram, the equilibrium phase for the composition of Mg–1.0Zn–0.33Ca (wt.%) at 300 °C is only α-Mg [19]. In addition to the segregation of Zn and Ca atoms at GBs, the introduction of precipitates with high thermostability, such as the MgSnCa phase with Sn to Ca weight ratio of 3:1, would further retard the grain growth during deformation [20, 21]. Note that the amount of Sn addition should be controlled at a low level to inhibit the formation of coarse MgSnCa phase. Trace Mn would be adopted to remove the Fe impurity and purify the Mg melt. When considering the amounts of alloying elements, the consumption of Ca by Sn should be taken in accounted, and thus a low-alloyed Mg–1.0Zn–0.45Ca–0.35Sn–0.2Mn (wt.%, ZXTM1000) alloy was designed. After hot rolling and annealing, the developed ZXTM1000 alloy exhibits high thermal stability during tension at 573 K and 1×10^{-3} s^{-1}, showing a good elongation to failure of ~410±30%. Moreover, the effects of solute segregation and precipitates on microstructural stability and superplastic deformation were discussed in detail.

2. Experimental procedures

A designed ZXTM1000 alloy was fabricated by melting pure Mg (99.90 wt. %), pure Zn (99.90 wt. %), pure Sn (99.90 wt. %), Mg–25Ca (wt. %), and Mg–5Mn (wt. %) in an electric furnace under a protective gas mixture of 99.5% CO_2 and 0.5% SF_6 at ~953 K. A homogenization treatment was conducted at 688 K for 24 h, followed by water quenching. After homogenization, the ingot was extruded at 703 K, with a ram speed of about 0.36 mm s^{-1} and an extrusion ratio of 35. The extruded plates were then hot-rolled at 573 K from ~5 mm to ~0.85 mm by 5 passes, with ~30% thickness reduction per pass. Afterward, the sheets were annealed at 523 K for 10 min, as denoted by the rolled and annealed ZXTM1000 alloy. Tensile specimens with a gauge dimension of 10 mm × 4 mm × 0.85 mm were machined from the annealed sheets along the rolling direction (RD).

The microstructure and microtexture were characterized by a scanning electron microscope (SEM) (TESCAN VEGA3 XMU, Czech) equipped with a NordlysNano EBSD detector, and a transmission electron microscope (TEM, JEM-2100F, Japan) operating at an accelerating voltage of 200 kV. Tensile tests at room temperature were carried out by an AGS-100 kN machine, and the strains were determined by video extensometer. The tensile tests at elevated temperatures were performed by an AGS-10 kN machine at 473K to 623 K and 1×10^{-4} s^{-1}–1×10^{-2} s^{-1}, and the elongations were calculated based on the displacement of the crosshead. For tensile tests at elevated temperatures, the samples were held for 10 min to reach the designated temperature before deformation. Tensile experiments in each condition were repeated at least three times to ensure the reliability of the experiment results. The atomic force microscopy (AFM, Multimode 8) was utilized to demonstrate the activation of GBS during deformation.

3. Results and discussion

Fig. 1a shows the tensile stress-strain curves of the rolled and annealed ZXTM1000 alloy tensioned at various temperatures and 1×10^{-3} s^{-1}. The low-alloyed ZXTM1000 alloy exhibits high yield strength of ~310 MPa and elongation to fracture of ~18% at room temperature (298 K). As expected, with the increase of temperature, the tensile elongation tends to increase first, and then decrease. Notably, the optimum superplasticity with elongation of ~410% was obtained when the ZXTM1000 alloy deformed at 573 K. Table 1 summarizes the elongations of the present ZXTM1000 alloy deformed at elevated temperatures and results for other Mg alloys with alloying content ≤ 4 wt. % in the literature are also included. Although the elongations of some Mg alloys subjected to SPD exceed that of the present study [7, 22], it is difficult to attain a superplastic elongation of over 400% by rolling or extrusion previously. Fig. 1c shows the plot of flow stress (ε = 0.1) as a function of strain rate at 573 K. The strain-rate sensitivity exponent (m) was calculated by $\partial log\sigma / \partial log\dot{\varepsilon}$, where σ is the flow stress, $\dot{\varepsilon}$ is the strain rate

Table 1
Elongations to failure of the present ZXTM1000 alloy after deformation at elevated temperatures as well as different strain rates, and correlated data of alloys with alloying content lower than 4 wt. % reported in the literature are also included.

Alloy	Processing	Grain size (μm)	Temperature (K)	Strain rate (s^{-1})	Elongation (%)	Refer-ence
ZXTM1000	Rolling	~4	473	1×10^{-3}	$\sim 80^{+5}_{-10}$	This study
			523		$\sim 180^{+10}_{-10}$	
			573		$\sim 410^{+30}_{-30}$	
			623		$\sim 210^{+10}_{-10}$	
			573	1×10^{-2}	$\sim 250^{+15}_{-15}$	
			573	2×10^{-2}	$\sim 300^{+15}_{-15}$	
			573	3×10^{-4}	$\sim 310^{+10}_{-20}$	
AZ31	Rolling	~6	573	1×10^{-4}	~350	[8]
AZ31	Extrusion	~2.5	523	1×10^{-3}	~300	[42]
AZ31	ECAP	~0.7	423	1×10^{-4}	~460	[42]
QE22	FSP	~0.6	723	1×10^{-2}	~1600	[22]
AZ31	ECAP	~2	623	1×10^{-4}	~700	[43]
ZK10	ECAP	~5	523	1×10^{-3}	~500	[7]

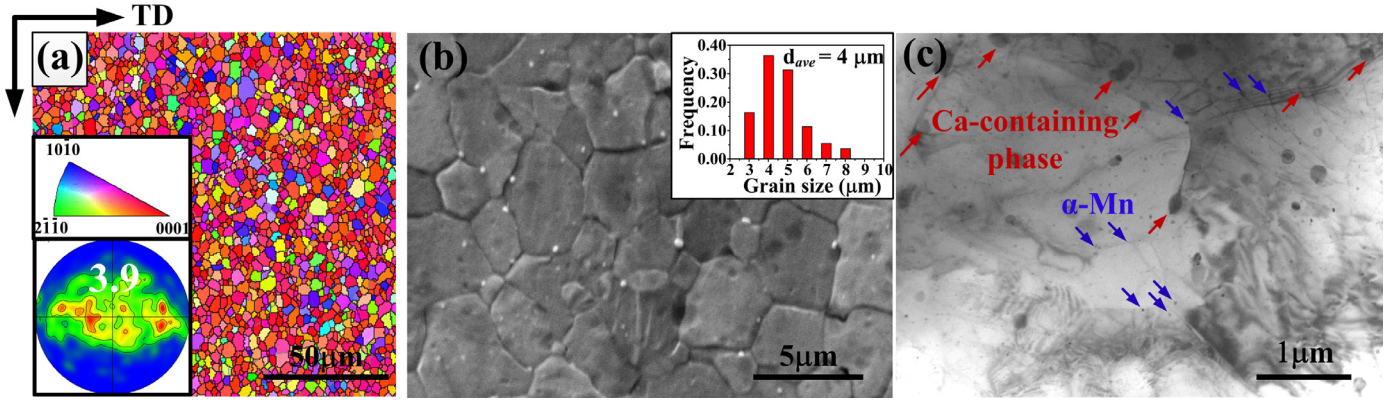

Fig. 2. (a) IPF map and 0001 pole figure, (b) SEM, and (c) BF-TEM images for the rolled and annealed ZXTM1000 alloy before tensile at 573 K.

[23]. The m value of $0.32^{+0.03}_{-0.03}$ at the strain rate ranging from 1×10^{-4} s^{-1} to 2×10^{-3} s^{-1} reveals a superplastic behavior dominated by GBS and solute drag creep (SDC) [24, 25].

The rolled and annealed ZXTM1000 alloy before tensioned at 573 K (have been kept in the high-temperature cabinet for 10 min) shows a uniform fine-grained structure with an average grain size of ~4 μm (Fig. 2a-b). The {0001} pole figure inserted in the IPF map exhibits a weakened basal texture with the maximum intensity of ~3.9 multiples of random distribution (Fig. 2a). A typical TEM image (Fig. 2c) shows that some Ca-containing phases sized in ~150 nm (indicated by the red arrows) and α-Mn phases (indicated by the blue arrows) sized in ~20 nm distribute near GBs, which are conducive to pinning GBs motion, and thus stabilize the microstructure.

To observe the microstructure evolution of the ZXTM1000 alloy during deformation at 573 K and 1×10^{-3} s^{-1}, IPF maps and corresponding {0001} pole figures were obtained from the gauge sections after strains of ~5%, ~100%, and ~200%. The gauge and grip sections of the fractured sample are also included. The initial fine equiaxed grain structure (Fig. 2a) keeps almost unchanged in the gauge section during the whole superplastic deformation (Fig. 3a-d), with a slightly increased average grain size of ~6 μm after fracture (Fig. 3d). Note that the grain size in the gauge section after fracture is smaller than that in the grip section (Fig. 3d and e), indicating a decelerated dynamic grain growth and meaning a superior thermostability of this low-alloyed ZXTM1000 alloy.

Fig. 4 shows high-angle annular dark-field (HAADF) images and corresponding EDS line-scanning results of the sample before deformation and after the strain of ~100%, showing evident segregation of Zn and Ca atoms at GBs. Previous studies [18, 26, 27] showed that the segregation of Zn and Ca atoms appeared both at the random boundary and special boundary, *i.e.* low (high) angle grain boundaries and isometric tilt grain boundaries, which indicates that the segregation of Zn and Ca atoms is independent of the grain boundary type. Note that compared to the undeformed sample (Fig. 4e and f), the extent of the co-segregation of Zn and Ca atoms at GBs decreases with the deformation processed (Fig. 4g and h), which is similar with reference [11, 28], leading to the weakening of stabilization effects (kinetically imposing a solute drag effect and thermodynamically decreasing the energy for grain growth) and even disappear. Thus, it can be concluded that the high thermal stability of the present ZXTM1000 alloy was provided by the co-segregation of Zn and Ca atoms at GBs coupled with precipitates, which is similar with reference [29].

As mentioned above, the superplastic deformation was co-dominated by GBS and SDC. Previous studies [30–32] showed that the AFM can be utilized to verify the occurrence of GBS via observing the sliding offsets (v) between the adjacent grains after deformation. In order to reduce the degree of oxidation, the sample after tensile elongation of ~25% at 573 K and 1×10^{-3} s^{-1} was selected, and the typical AFM topology map is shown in Fig. 5a. The height along with Line A, B, and C crossing 3 individual GBs (Fig. 5a) was quantified, and the profiles are presented in Fig. 5b. One can see that the value of v varies with the sample position and the value can reach ~470 nm, indicating that the GBS accommodated the deformation in an inhomogeneous manner. The {0001} pole figures inserted in IPF maps (Fig. 3) show that the basal texture becomes stronger gradually as tensile proceeds at later deformation stage, implies the active dislocation movement [25, 33]. Fig. 6 shows the TEM characterization of the ZXTM1000 alloy after a strain of ~100%, and most of the dislocations (Fig. 6a) tend to be parallel and sweep across the grain interior (indicated by the black, blue, and green lines). BF-STEM image (Fig. 6b) shows that some dislocations are attached to the second phases (indicated by the red arrows), showing

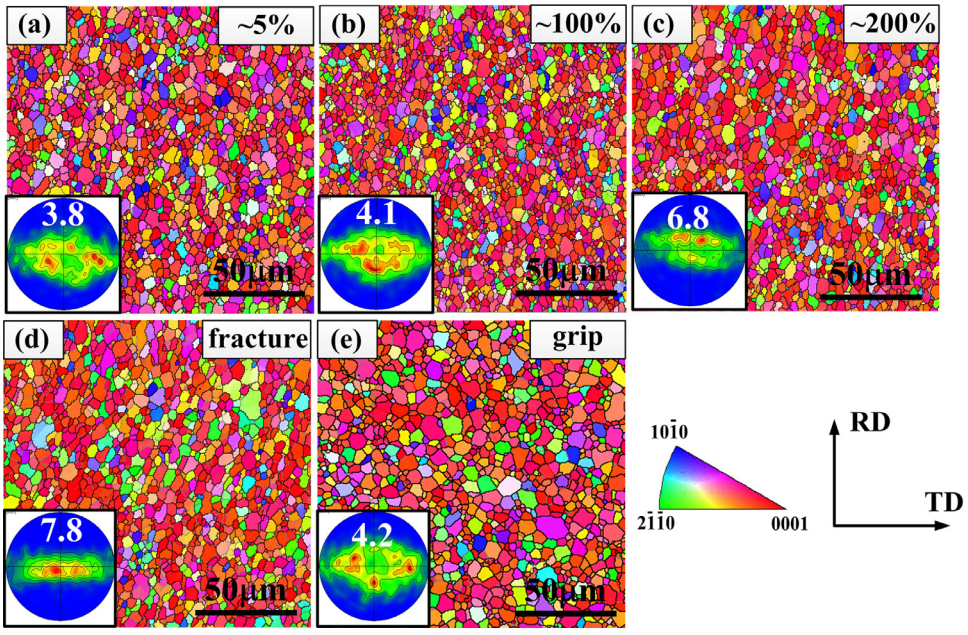

Fig. 3. IPF maps and {0001} pole figures of the gauge sections after (a) ~5% elongation, (b) ~100% elongation, (c) ~200% elongation, (d) fracture at 573 K and 1×10^{-3} s^{-1}, as well as (e) the grip section of the fractured sample.

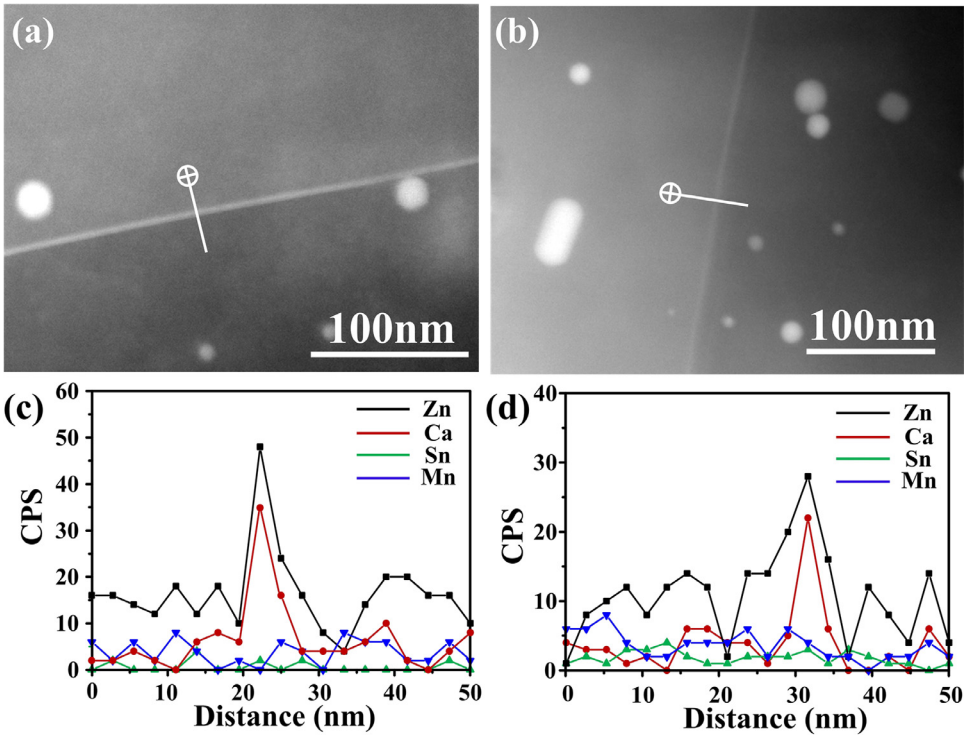

Fig. 4. (a, b) HAADF-STEM images and (c, d) corresponding line EDS scanning results of the rolled and annealed ZXTM1000 alloy (a, c) before tension, and (b, d) after tensile elongations of ~100% at 573 K and 1×10^{-3} s^{-1}.

a possibility to climb over the particles during deformation [34, 35]. The above distinct characteristics, related to the lattice dislocation activity and configurations, reveal the phenomenon of viscous glide of dislocations in the grain [34, 35]. Previous study [36] also pointed out that solute atoms may segregate preferentially around the dislocations during deformation at elevated temperatures, causing a dragging force that interacts with moving dislocations, and thus the dislocations viscous glide become the rate-controlling mechanism. Therefore, the GBS and SDC are mainly responsible for the superplastic tensile deformation in the present study.

Note that the examined m value ($0.32^{+0.03}_{-0.03}$) in the present ZXTM1000 alloy during superplastic flow was lower than the general value (~0.5) for conventional superplasticity and it may be a consequence of the existence of a threshold stress. Conventionally, a plot of $\sigma - \dot{\varepsilon}^{1/n}$ (where $n = 1/m$) was used to predict the threshold stress, which is estimated by an extrapolation of the data when the strain rate is zero with a linear regression [24]. The calculated value of the threshold stress is ~4 MPa at 573 K (Fig. 1d). Mohamed *et al.* [34, 35, 37] systematically investigated the threshold stress behavior during superplastic deformation. They pointed out that the threshold stress is likely originated from the pinning effect exerted on dislocations by solute segregation either at GBs or around precipitates within the grains. In the present study, the Ca atoms with a bigger atomic radius (0.197 nm) than Mg atom (0.160 nm) tend to segregate to the tensile stress field region around the disloca-

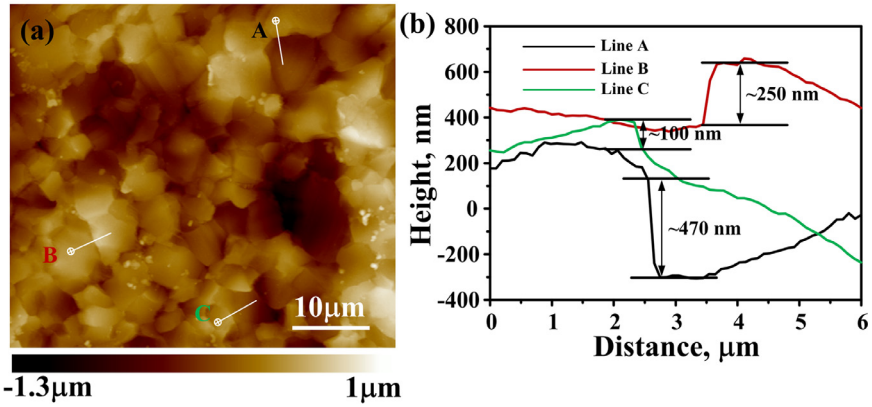

Fig. 5. (a) AFM topology map obtained from the rolled and annealed ZXTM1000 alloy after tensile elongation of ~25% at 573 K and 1×10^{-3} s^{-1}, (b) height profile along with Line A, B, and C in (a).

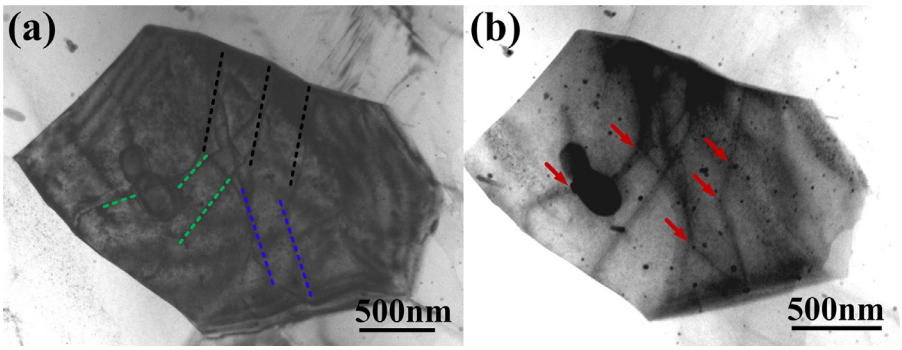

Fig. 6. (a) TEM and (b) BF-STEM images of the rolled and annealed ZXTM1000 alloy after tensile elongation of ~100% at 573 K and 1×10^{-3} s^{-1}.

tions at GBs, while the smaller Zn atoms (0.134 nm) incline to diffuse to the compression region [16]. Such co-segregation would cause a strong pinning effect on the moving dislocations, leading to the presence of a threshold stress, and thus hindering the operation of GBS during deformation. However, the positive effects in accommodating deformation brought by the co-segregation of Zn and Ca atoms would exceed the negative effects of impeding GBS, which would be discussed in detail later.

Although the superplastic deformation co-dominated by GBS and SDC is often observed in low-alloyed Mg alloys [38, 39], the elongation exceeding 400% has rarely been reported in the rolled/extruded Mg alloys. The most important reason for that is less contribution from GBS due to initial coarse grains or the grain coarsening during deformation. One can see that a uniform fine-grained ($d < 6$ μm) microstructure was retained attributed by the co-segregation of Zn and Ca atoms and precipitates at GBs during deformation, which leads to an enhanced GBS [40]. Wu et al. [39] also reported that for a AZ31 alloy deformed at 643 K and 4×10^{-3} s^{-1}, although the value of m is only 0.27, a fine-grained microstructure ($d < 10$ μm) during deformation favors the active operation of GBS to dominant deformation. Furthermore, near-equiaxed fine grains with uniform distribution would exhibit good deformation compatibility, and thus minimizing void formation and coalescence during superplastic deformation, leading to a larger elongation to failure.

It was reported that a non-equilibrium GB containing long-range stresses would hamper the process of relieving stress localization arising from the process of GBS [41]. In the present study, the co-segregation of Zn and Ca atoms at GBs existed during deformation, decreasing the elastic strain energy of GBs and relieving the local stress concentration, which favors GBS. Note that the degradation of the co-segregation of Zn and Ca atoms at GBs occurs during the superplastic tensile deformation (Fig. 4). This behavior may be attributed to the diffusion behavior of the pre-existing Zn-Ca segregation at GBs, indicating an active operation of local diffusional process to accommodate deformation. Therefore, it is feasible to achieve superplasticity in low-alloyed Mg alloys when the microstructure of the alloy is co-stabilized by solute segregation at GBs and precipitates.

A benchmark sample, which was further annealed at 573 K for 30 min to eliminate the content of co-segregation of Zn and Ca atoms at GBs after rolling and annealing at 523 K for 10 min, was select to tension at 573 K and 1×10^{-3} s^{-1}. Fig. 7a shows the tensile stress-strain curve of the benchmark sample, and the result of the rolled and annealed ZXTM1000 alloy is also included for comparison. The benchmark sample exhibits a superplastic elongation of ~300%, significantly lower than that of the rolled and annealed ZXTM1000 alloy about 110%. The benchmark sample before tension presents similar grain size distribution and weakened basal texture with the rolled and annealed ZXTM1000 alloy (Fig. 7b), which eliminates the effects of initial grain size and texture on superplasticity. The BF-TEM image (Fig. 7c) also shows some Ca-containing phases and α-Mn phases locate at GBs, which is similar to the rolled and annealed ZXTM1000 alloy. Therefore, it is rather safe to say that the difference in elongations between the two alloys originates from the co-segregation of Zn and Ca atoms at GBs.

To examine the effect of strain rate on the superplasticity, tensile tests at 573 K were also performed on the rolled and annealed ZXTM1000 alloys at the strain rate ranging from 3×10^{-4} s^{-1} to 1×10^{-2} s^{-1}. Since GBS is considered as a diffusion process that is greatly susceptible to GBs diffusion, the reduction of strain rate would be accompanied by an increased possibility for the occurrence of GBS, and thus enhancing the superplastic elongation. However, the tensile elongation for the strain rate 3×10^{-4} s^{-1} (~310%, Fig. 1b) is lower than that when tensioned at 1×10^{-3} s^{-1} (~410%, Fig. 1a), which can be attributed to an increased exposure time at 573 K. The extension of exposure time at high temperature degrades the stabilized effects derived from the co-segregation of Zn and Ca and precipitates at GBs, and then the grain coarsening occurred, offsetting the advantages provided by the decreased strain rate and deteriorating the ability of superplastic deformation. Moreover, the high-strain-rate superplasticity (~250% at 573 K and 1×10^{-2} s^{-1}, Fig. 1b) are not impressive, implying a further

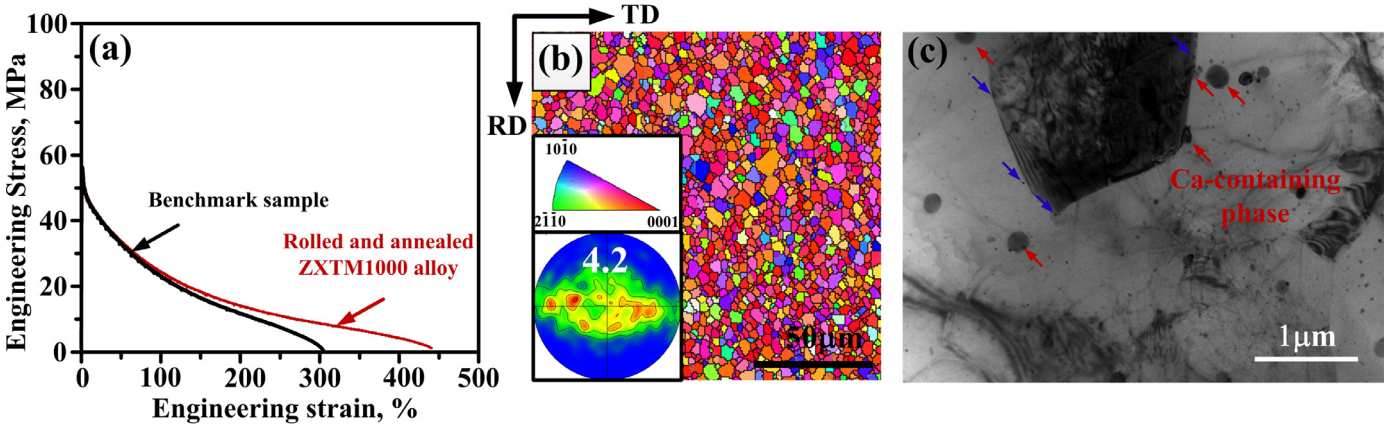

Fig. 7. (a) Tensile stress-strain curves of the benchmark sample and the rolled and annealed ZXTM1000 alloy deformed at 573 K and 1×10^{-3} s^{-1}; (b) IPF map and (c) BF-TEM image for the benchmark sample.

study still needs to be done. Nevertheless, this work offers a strategy of solute segregation at GBs coupled with precipitates to stabilize the microstructure of Mg alloys during deformation at elevated temperatures, which provides a new path for alloy design and achieving superplasticity, and thus broadening the dilute Mg alloys application of superplastic forming in the fabrication of complex products, such as the body shell of computer.

4. Conclusion

In summary, a low-alloyed ZXTM1000 alloy sheet, with the co-segregation of Zn and Ca atoms at GBs, exhibited a superior elongation of ~410% at 573 K and 1×10^{-3} s^{-1}, which is ~110% larger than that of the benchmark sample. The superplastic deformation was accommodated by GBS and SDC. The initial fine-grained structure of the rolled and annealed ZXTM1000 alloy was only undergone a slight growth from ~4 μm to ~6 μm during deformation, which is benefited from the synergistic stabilization mechanisms induced by the co-segregations at GBs and precipitates. The solute segregations at GBs are not conducive to the operation of GBS due to the existence of a threshold stress (~4 MPa). However, the resulting superior thermostability is of great advantage for accommodating deformation at elevated temperatures, which makes the present ZXTM1000 alloy distinct from other low-alloyed Mg alloys.

Declaration of Competing Interest

The authors declare that they have no known competing financial interests or personal relationships that could have appeared to influence the work reported in this paper.

Acknowledgments

Financial supports from The National Natural Science Foundation of China (Nos. 51625402, U19A2084 and 51801069) are greatly acknowledged. Partial financial support came from The Science and Technology Development Program of Jilin Province (Nos. 20200401025GX and 20200201002JC), Program for JLU Science and Technology Innovative Research Team (JLUSTIRT, 2017TD-09), and The Changjiang Scholars Program (T2017035).

Reference

[1] W.J. Kim, I.K. Moon, S.H. Han, Ultrafine-grained Mg–Zn–Zr alloy with high strength and high-strain-rate superplasticity, Mater. Sci. Eng. A 538 (2012) 374–385, doi:10.1016/j.msea.2012.01.063.
[2] W.J. Kim, I.B. Park, Enhanced superplasticity and diffusional creep in ultrafine-grained Mg–6Al–1Zn alloy with high thermal stability, Scr. Mater. 68 (2013) 179–182, doi:10.1016/j.scriptamat.2012.10.011.
[3] L.H. Wu, P. Xue, B.L. Xiao, Z.Y. Ma, Achieving superior low-temperature superplasticity for lamellar microstructure in nugget of a friction stir welded Ti-6Al-4V joint, Scr. Mater. 122 (2016) 26–30, doi:10.1016/j.scriptamat.2016.05.020.
[4] Hang Zhang, Huiyuan Wang, Xinyu Xu, Min Zha, Cheng Wang, Pinkui Ma, Zhiping Guan, Current research and future prospect on microstructure stability of superplastic light alloys, Acta Metall Sin. 54 (2018) 1618–1624, doi:10.11900/0412.1961.2018.00391.
[5] M. Zha, H.-M. Zhang, C. Wang, H.-Y. Wang, E.-B. Zhang, Q.-C. Jiang, Prominent role of a high volume fraction of $Mg_{17}Al_{12}$ particles on tensile behaviors of rolled Mg–Al–Zn alloys, J. Alloys Compd 728 (2017) 682–693, doi:10.1016/j.jallcom.2017.08.289.
[6] R.B. Figueiredo, S. Terzi, T.G. Langdon, Using X-ray microtomography to evaluate cavity formation in a superplastic magnesium alloy processed by equal-channel angular pressing, Acta Mater. 58 (2010) 5737–5748, doi:10.1016/j.actamat.2010.06.049.
[7] R.B. Figueiredo, T.G. Langdon, Achieving superplastic properties in a ZK10 magnesium alloy processed by equal-channel angular pressing, J. Mater. Res. Technol. 6 (2017) 129–135, doi:10.1016/j.jmrt.2016.05.005.
[8] S.S. Park, G.T. Bae, D.H. Kang, B.S. You, N.J. Kim, Superplastic deformation behavior of twin-roll cast Mg–6Zn–1Mn–1Al alloy, Scr. Mater. 61 (2009) 223–226, doi:10.1016/j.scriptamat.2009.03.057.
[9] X.H. Shao, Q.Q. Jin, Y.T. Zhou, H.J. Yang, S.J. Zheng, B. Zhang, Q. Chen, X.L. Ma, Segregation of solute atoms along deformation-induced boundaries in an Mg–Zn–Y alloy containing long period stacking ordered phase, Materialia 6 (2019) 100287, doi:10.1016/j.mtla.2019.100287.
[10] X.H. Shao, Z.Z. Peng, Q.Q. Jin, X.L. Ma, Atomic-scale segregations at the deformation-induced symmetrical boundary in an Mg-Zn-Y alloy, Acta Mater. 118 (2016) 177–186, doi:10.1016/j.actamat.2016.07.054.
[11] M.M. Hoseini-Athar, R. Mahmudi, R.P. Babu, P. Hedström, Effect of Zn content on the microstructural stability and grain growth kinetics of fine-grained extruded Mg–Gd–Zn alloys, J. Alloys Compd. 831 (2020) 154766, doi:10.1016/j.jallcom.2020.154766.
[12] J.D. Robson, Effect of rare-earth additions on the texture of wrought magnesium alloys: the role of grain boundary segregation, Metall. Mater. Trans. A 45 (2013) 3205–3212, doi:10.1007/s11661-013-1950-1.
[13] X.C. Cai, B.R. Sun, Y. Liu, N. Zhang, J.H. Zhang, H. Yu, J.Y. Huang, Q.M. Peng, T.D. Shen, Selection of grain-boundary segregation elements for achieving stable and strong nanocrystalline Mg, Mater. Sci. Eng. A 717 (2018) 144–153, doi:10.1016/j.msea.2018.01.058.
[14] J. Hu, Y.N. Shi, X. Sauvage, G. Sha, K. Lu, Grain boundary stability governs hardening and softening in extremely fine nanograined metals, Science 355 (2017) 1292, doi:10.1126/science.aal5166.
[15] P. Choi, M. Dasilva, U. Klement, T. Alkassab, R. Kirchheim, Thermal stability of electrodeposited nanocrystalline Co-1.1at.%P, Acta Mater. 53 (2005) 4473–4481, doi:10.1016/j.actamat.2005.06.006.
[16] Z.R. Zeng, Y.M. Zhu, S.W. Xu, M.Z. Bian, C.H.J. Davies, N. Birbilis, J.F. Nie, Texture evolution during static recrystallization of cold-rolled magnesium alloys, Acta Mater. 105 (2016) 479–494, doi:10.1016/j.actamat.2015.12.045.
[17] T.T.T. Trang, J.H. Zhang, J.H. Kim, A. Zargaran, J.H. Hwang, B.C. Suh, N.J. Kim, Designing a magnesium alloy with high strength and high formability, Nat. Commun. 9 (2018) 2522, doi:10.1038/s41467-018-04981-4.
[18] M.Z. Bian, T.T. Sasaki, T. Nakata, Y. Yoshida, N. Kawabe, S. Kamado, K. Hono, Bake-hardenable Mg–Al–Zn–Mn–Ca sheet alloy processed by twin-roll casting, Acta Mater. 158 (2018) 278–288, doi:10.1016/j.actamat.2018.07.057.
[19] K. Oh-ishi, R. Watanabe, C.L. Mendis, K. Hono, Age-hardening response of Mg–0.3at.%Ca alloys with different Zn contents, Mater. Sci. Eng. A 526 (2009) 177–184, doi:10.1016/j.msea.2009.07.027.
[20] Y. Chai, B. Jiang, J. Song, Q. Wang, H. Gao, B. Liu, G. Huang, D. Zhang, F. Pan, Improvement of mechanical properties and reduction of yield asymmetry of extruded Mg-Sn-Zn alloy through Ca addition, J. Alloys Compd. 782 (2019) 1076–1086, doi:10.1016/j.jallcom.2018.12.109.

[21] H. Pan, G. Qin, M. Xu, H. Fu, Y. Ren, F. Pan, Z. Gao, C. Zhao, Q. Yang, J. She, B. Song, Enhancing mechanical properties of Mg–Sn alloys by combining addition of Ca and Zn, Mater. Des. 83 (2015) 736–744, doi:10.1016/j.matdes.2015.06.032.
[22] F.K. Md, S.K. Panigrahi, Achieving excellent superplasticity in an ultrafine-grained QE22 alloy at both high strain rate and low-temperature regimes, J. Alloys Compd. 747 (2018) 71–82, doi:10.1016/j.jallcom.2018.02.294.
[23] H.-M. Zhang, X.-M. Cheng, M. Zha, Y.-K. Li, C. Wang, Z.-Z. Yang, J.-G. Wang, H.-Y. Wang, A superplastic bimodal grain-structured Mg–9Al–1Zn alloy processed by short-process hard-plate rolling, Materialia 8 (2019) 100443, doi:10.1016/j.mtla.2019.100443.
[24] V. Jain, R.S. Mishra, R. Verma, E. Essadiqi, Superplasticity and microstructural stability in a Mg alloy processed by hot rolling and friction stir processing, Scr. Mater. 68 (2013) 447–450, doi:10.1016/j.scriptamat.2012.11.009.
[25] T.R. McNelley, K. Oh-Ishi, A.P. Zhilyaev, S. Swaminathan, P.E. Krajewski, E.M. Taleff, Characteristics of the transition from grain-boundary sliding to solute drag creep in superplastic AA5083, Metall. Mater. Trans. A 39 (2007) 50–64, doi:10.1007/s11661-007-9401-5.
[26] Z.R. Zeng, Y.M. Zhu, J.F. Nie, S.W. Xu, C.H.J. Davies, N. Birbilis, Effects of calcium on strength and microstructural evolution of extruded alloys based on Mg–3Al–1Zn–0.3Mn, Metall. Mater. Trans. A 50 (2019) 4344–4363, doi:10.1007/s11661-019-05318-6.
[27] Y.M. Zhu, J.F. Nie, Springer International Publishing, Cham, 2019, pp. 263–266.
[28] M. Sanjari, A.R. Farkoosh, B. Shalchi Amirkhiz, Y. He, A. Javaid, A.S. Kabir, J. Su, I.-H. Jung, S. Yue, The role of the Zn/Nd ratio in the microstructural evolution of the Mg-Zn-Nd system during static recrystallization: Grain boundary partitioning of solutes, Scr. Mater. 134 (2017) 1–5, doi:10.1016/j.scriptamat.2017.01.033.
[29] A. Devaraj, W. Wang, R. Vemuri, L. Kovarik, X. Jiang, M. Bowden, J.R. Trelewicz, S. Mathaudhu, A. Rohatgi, Grain boundary segregation and intermetallic precipitation in coarsening resistant nanocrystalline aluminum alloys, Acta Mater. 165 (2019) 698–708, doi:10.1016/j.actamat.2018.09.038.
[30] B. Kim, J.C. Kim, S. Lee, K.-S. Lee, J.G. Lee, S.S. Park, High-strain-rate superplasticity of fine-grained Mg–6Zn–0.5Zr alloy subjected to low-temperature indirect extrusion, Scr. Mater. 141 (2017) 138–142, doi:10.1016/j.scriptamat.2017.08.008.
[31] J.H. Han, F.A. Mohamed, Quantitative measurements of grain boundary sliding in an ultrafine-grained Al alloy by atomic force microscopy, Metall. Mater. Trans. A 42 (2011) 3969–3978, doi:10.1007/s11661-011-0871-0.
[32] K. Edalati, Z. Horita, R.Z. Valiev, Transition from poor ductility to room-temperature superplasticity in a nanostructured aluminum alloy, Sci. Rep. 8 (2018) 6740, doi:10.1038/s41598-018-25140-1.
[33] R. Panicker, A.H. Chokshi, R.K. Mishra, R. Verma, P.E. Krajewski, Microstructural evolution and grain boundary sliding in a superplastic magnesium AZ31 alloy, Acta Mater. 57 (2009) 3683–3693, doi:10.1016/j.actamat.2009.04.011.
[34] Y. Xun, F.A. Mohamed, Superplastic behavior of Zn–22%Al containing nano-scale dispersion particles, Acta Mater. 52 (2004) 4401–4412, doi:10.1016/j.actamat.2004.03.039.
[35] F.A. Mohamed, On the origin of superplastic flow at very low stresses, Mater. Sci. Eng. A 410-411 (2005) 89–94, doi:10.1016/j.msea.2005.08.004.
[36] T.G. Langdon, Grain boundary sliding revisited: Developments in sliding over four decades, J. Mater. Sci. 41 (2006) 597–609, doi:10.1007/s10853-006-6476-0.
[37] F.A. Mohamed, Interpretation of superplastic flow in terms of a threshold stress, J. Mater. Sci. 18 (1983) 582–592, doi:10.1007/BF00560647.
[38] H. Watanabe, H. Tsutsui, T. Mukai, M. Kohzu, S. Tanabe, K. Higashi, Deformation mechanism in a coarse-grained Mg–Al–Zn alloy at elevated temperatures, Int. J. Plast. 17 (2001) 387–397, doi:10.1016/S0749-6419(00)00042-5.
[39] H.-y. Wu, W.-c. Hsu, Tensile flow behavior of fine-grained AZ31B magnesium alloy thin sheet at elevated temperatures, J. Alloys Compd. 493 (2010) 590–594, doi:10.1016/j.jallcom.2009.12.162.
[40] J. Victoria-Hernandez, S. Yi, D. Letzig, D. Hernandez-Silva, J. Bohlen, Microstructure and texture development in hydrostatically extruded Mg–Al–Zn alloys during tensile testing at intermediate temperatures, Acta Mater. 61 (2013) 2179–2193, doi:10.1016/j.actamat.2012.12.039.
[41] M. Mabuchi, K. Ameyama, H. Iwasaki, K. Higashi, Low temperature superplasticity of AZ91 magnesium alloy with non-equilibrium grain boundaries, Acta Mater. 47 (1999) 2047–2057, doi:10.1016/S1359-6454(99)00094-4.
[42] H.K. Lin, J.C. Huang, T.G. Langdon, Relationship between texture and low temperature superplasticity in an extruded AZ31 Mg alloy processed by ECAP, Mater. Sci. Eng. A 402 (2005) 250–257, doi:10.1016/j.msea.2005.04.018.
[43] R.B. Figueiredo, T.G. Langdon, Developing superplasticity in a magnesium AZ31 alloy by ECAP, J. Mater. Sci. 43 (2008) 7366–7371, doi:10.1007/s10853-008-2846-0.